New BIOTECHNOLOGY 93 (2026) 316–324

Contents lists available at ScienceDirect

New BIOTECHNOLOGY

journal homepage: www.elsevier.com/locate/nbt

# Photosynthetic engineered living materials incorporating recombinant *Chlamydomonas reinhardtii* enable long-term semi-continuous photobiotransformation

Vilja Siitonen [a], Tiia Siivola [a,1], Pornpan Napaumpaiporn [a], Tekla Tammelin [b], Yagut Allahverdiyeva [a,*]

[a] *Molecular Plant Biology, Department of Life Technologies, University of Turku, Turku 20014, Finland*
[b] *VTT Technical Research Centre of Finland Ltd, VTT, PO Box 1000, Espoo FI-02044, Finland*

ARTICLE INFO

*Keywords:*
*Chlamydomonas reinhardtii*
Cyclohexanone monooxygenase (CHMO)
Baeyer-Villiger monooxygenase BVMO
Alginate
TEMPO-oxidized cellulose nanofibers (TCNF)
Immobilization
Engineered living materials

ABSTRACT

Photosynthetic engineered living materials (ELMs) present an attractive platform for producing valuable compounds and fuels using solar energy. Compared to traditional suspension cultures, ELMs enable long-term biocatalytic activity, more efficient light utilization, and facilitate downstream processing. In this study, we developed photosynthetic ELMs by entrapping *Chlamydomonas reinhardtii* in either alginate or TEMPO-oxidized cellulose nanofibers (TCNF). The strain utilized was converting cyclohexanone to ε-caprolactone via photobiotransformation. The cell loading and matrix material were evaluated in short-term reactions and during a semi-continuous bioproduction in vials. We showed that the entrapped cells remain photosynthetically active and catalytically competent over extended periods. By replenishing the substrate and collecting the product every 24 h we achieved semi-continuous photobiotransformation for over two weeks, reaching an average productivity of 2.31 ± 0.26 g $m^{-2}$ $d^{-1}$ and accumulating 0.31 ± 0.03 mol $m^{-2}$ corresponding to 3.49 ± 0.31 g $L^{-1}$ of ε-caprolactone. These findings establish photosynthetic ELMs as a viable approach for long-term whole-cell photobiotransformation.

## 1. Introduction

Developing sustainable strategies for chemicals and fuels production is at the core of the green transition. One promising approach is harnessing photosynthetic organisms as biocatalysts in whole-cell biotransformation, because they can couple the conversion of an externally supplied substrates to value-added desired products with their inherent capacity to produce molecular oxygen and reducing equivalents through photosynthesis [1,2]. This photodriven supply of redox equivalents reduces the dependency on organic feedstocks. Both native [3] and engineered strains of cyanobacteria and microalgae [4–8] have been successfully applied for photosynthetic whole-cell biotransformation. These microorganisms can host a broad range of heterologous oxidoreductases, monooxygenases and P450 enzymes, enabling light driven oxygenation, hydroxylation, reduction reactions [5,8–11]. Whole microbial cells provide a protective and self-regenerating environment for enzymatic activity, thereby enhancing enzyme stability, supporting cofactor regeneration and enabling prolonged catalytic function. Additionally, these photosynthetic cells can be cultivated in environmentally friendly mild conditions, and the biocatalytic processes are scalable [12] - an essential factor for industrial applications.

Baeyer–Villiger monooxygenases (BVMOs) are an important FAD-dependent class of enzymes used in whole-cell biotransformation to oxygenate ketones, aldehydes or heteroatoms [13,14]. These enzymes require both NAD(P)H and molecular oxygen to perform their catalytic function [15,16]. BVMOs have been expressed in heterotrophic hosts, e.g. *Escherichia coli*, and have been explored for long-term biotransformation processes. However, these efforts are typically limited by cofactor regeneration, restricting the reaction time to approximately 40 h [17]. As a promising alternative, oxygenic photosynthetic microorganisms serve as a highly effective whole-cell biocatalysts, offering a continuous supply of oxygen and regenerating essential cofactors through photosynthesis [5,6,8]. Recently, a fed-batch biotransformation using engineered *Synechocystis* sp. PCC6803 (*Synechocystis* thereafter)

* Corresponding author.
*E-mail address:* allahve@utu.fi (Y. Allahverdiyeva).
[1] Present address: Department of Bioproducts and Biosystems, Aalto University School of Chemical Engineering, Espoo, Aalto FI-00076, Finland

https://doi.org/10.1016/j.nbt.2026.04.004
Received 16 June 2025; Received in revised form 31 January 2026; Accepted 20 April 2026
Available online 21 April 2026

expressing a BVMO was demonstrated in 2-liter fed-batch suspension cultures operated for 27 h [18]. This process was extended to a 48-hour coupled reaction, yielding 3.11 ± 0.12 g $L^{-1}$ of 6-hydroxyhexanoic acid [19].

While suspension cultures enable efficient light-driven biotransformation, increasing culture density to enhance productivity introduces substantial challenges. A key limitation is self-shading, where high cell densities hinder light penetration, thereby reducing photosynthetic efficiency [20]. This challenge can be partly mitigated using photobioreactors with short light-paths [21–24]. Another limitation of suspension cultures is separating cells from the reaction medium, especially when the cells would be used for multiple rounds of biotransformation cycles. In natural environments, microbial cells often form biofilms, which are mechanically robust and can persist for prolonged time [25]. By mimicking these natural biofilms via immobilizing cells within various synthetic or bio-based matrices possessing properties such as transparency, biocompatibility, mechanical stability, and porosity, has emerged as an alternative approach to tackle these challenges [26–29]. Although immobilization of cells can decrease biocatalytic efficiency due to mass transfer limitations [9], the higher process stability and reusability often lead to higher overall product yields over extended operational periods [30,31].

In this study, we present a proof-of-concept for utilizing thin-film immobilized *Chlamydomonas reinhardtii* (*Chlamydomonas* hereafter) as photosynthetic engineered living materials (ELMs) for sustained, semi-continuous photobiotransformation cycles. We immobilized a recombinant *Chlamydomonas* expressing a cyclohexanone monooxygenase from *Acinetobacter* [8] in two bio-based, transparent hydrogel matrices [32,33]. - The first, alginate, is a linear polymer formed by 1,4-glycosidic linkages between two types of monomer subunits, α-L-guluronic acid and β-D-mannuronic acid [34] and capable of forming $Ca^{2+}$-crosslinked hydrogels [33]. The second matrix material is TEMPO-oxidized cellulose nanofibers (TCNF), composed of chemically modified cellulose nanofibers with carboxylic groups that enable the formation of optically transparent hydrogels [35]. Using these materials, we assessed both short-term photobiotransformation and multiple consecutive 24-h cycles to achieve a semi-continuous production of ε-caprolactone. Notably, alginate-based ELMs remain functional for over 16 consecutive cycles, highlighting their robustness for prolonged biocatalytic operation.

## 2. Materials and methods

### 2.1. Strain and growth conditions

Recombinant *Chlamydomonas reinhardtii* (UVM11-CW/CHMO_PSAD) expressing $CHMO_{Acinetobacter}$ and targeted to the chloroplast with the PSAD transit peptide [8], was used in this study. All cultures were grown and maintained in Tris-acetate-phosphate (TAP) medium, pH 7.2 [36] under 35 μmol $m^{-2}$ $s^{-1}$ photosynthetically active radiation (PAR) provided by a fluorescent lamp (Philips Master TL-D 36 W/865, the Netherlands) at + 25°C, with ambient air and continuous shaking at 120 rpm in growth chamber (MIR-S100, Sanyo, Japan). *Chlamydomonas* stock- and pre-cultures were supplemented with 100 μg $ml^{-1}$ spectinomycin (Sigma Aldrich, China). For all experiments, a 40 ml pre-culture was prepared by inoculating 0.5 ml of stock culture and grown for three days prior to use. Experimental cultures for immobilization were inoculated at 1% (v/v) from pre-cultures into fresh TAP medium (without antibiotics) and grown for three days until reaching $OD_{750}$ ~1.2–1.4. The cells were harvested by centrifugation at 3 000 x g for 5 min, washed with TAP, pelleted and used for further experiments.

### 2.2. Immunological detection of the heterologously expressed CHMO

Approximately 5*$10^7$ *Chlamydomonas* cells were harvested each day. For day 0, cells from the pre-culture were used. Sample preparation was performed as described in [37], with minor modifications: 5% (w/v) SDS and 30% (w/v) sucrose were used. Total protein corresponding to 1 μg Chl was separated on a 12% SDS-PAGE gel, transferred onto a PVDF membrane (Immobilon, Merck). Immunodetection was performed using a primary mouse anti-HA antibody (Sigma Aldrich, USA) followed by a secondary AP-Goat Anti-Mouse IgG (H+L) Conjugate (Zymed, USA). Signal development was done using Fuji Medical X-ray films (Fujifilm, Japan). After immunodetection membranes were stained with Coomassie Brilliant Blue (Bio-Rad, United Kingdom) to confirm equal protein load. Three biological replicates were analyzed.

Statistical significance was assessed using a two-tailed Student's *t*-test assuming equal variance. Multiple comparisons were corrected using the Benjamini-Hochberg False Discovery Rate (FDR) method to control for Type I errors.

For the immunological detection of CHMO from the films, samples were collected at days 0, 5, 12 and 19 after start of the biotransformation and subsequently frozen for later use. The films were then dissolved in 50 mM ethylenediaminetetraacetic acid (EDTA), pH 7.0 and processed in the same manner as the suspension samples, with the exception that protein separation was performed using 4–15% Mini-Protean TGX precast protein gels (Bio-Rad).

### 2.3. Fabrication of ELMs with Chlamydomonas

#### 2.3.1. Producing Alginate-ELM (Alg-ELM) with immobilized Chlamydomonas

Setup A1-Alg-ELM is the default that has been used for alginate films with *Synechocystis* cells before [29]. The immobilization mixture was prepared using a ratio of 1 g wet cell weight: 0.5 ml $H_2O$: 1 ml 4% (w/v) alginate (alginic acid sodium salt from brown algae, Sigma Aldrich, Norway) leading to a final alginate concentration of 2% (w/v) in the film. Mixture was spread on an immobilization scaffold to ~450 μm thickness using either a 3D-printed polylactic acid (PLA) mesh, a 3D-printed polyethylene terephthalate (PET) mesh, or a plasmonated polytetrafluoroethylene (PTFE) film (Etra, Finland). The films were then sprayed with 50 mM $CaCl_2$ (Sigma Aldrich, Japan) and incubated for 20 min, followed by wash with Milli-Q water and cutting into 3 × 1 cm strips. For photobiotransformation experiments, three biological replicates were used, each consisting of 3–5 technical replicates.

Setup A2-Alg-ELM was prepared with a lower cell density. *Chlamydomonas* cells were resuspended in 20–40 ml of TAP medium and the immobilization mixture was adjusted to a final concentration of 1 mg $ml^{-1}$ of Chl in 1% (w/v) alginate. Alg-ELM mixture was spread on a PTFE film (either plasmonated or heat treated between glass plates to get a flat surface film) to a thickness of 450 μm. The hydrogels were sprayed with 50 mM $CaCl_2$, incubated for 20 min, cut out into 3 × 1 strips, and submerged in 50 mM $CaCl_2$ for 15 min. ELMs were then incubated for 3 days at 25°C under 20 μmol $m^{-2}$ $s^{-1}$ PAR in ambient air. For photobiotransformation experiments, three biological replicates were used, each with three technical replicates.

#### 2.3.2. Fabrication of TCNF-ELM with immobilized Chlamydomonas

Immobilization mixture contained cells adjusted to 1 mg $ml^{-1}$ of Chl, 0.5% (w/v) TEMPO-oxidized cellulose nanofibers, which had been manufactured from never-dried softwood kraft pulp that was obtained from a coniferous wood mixture consisting of spruce and pine. Pulping was carried out in a Finnish pulp mill and the TEMPO-catalyzed oxidation of the pulp was conducted with alkaline hypochlorite as the primary oxidant according to the protocol reported in [38] and 0.1% (w/v) polyvinyl alcohol (PVA) [35]. The mixture was homogenized with T25 digital Ultra-Turrax homogenizer (IKA, Staufen, Germany) at 12 000 rpm for 1.5 min and then centrifuged at 3 000 x g for 3 min. Mixture was spread on plasmonated PTFE film to a thickness of 450 μm. The TCNF-ELM was sprayed with 50 mM $CaCl_2$, incubated for 20 min, and dried to 50% moisture content. Afterwards, the TCNF-ELMs were cut into 3 × 1 cm strips and submerged into 50 mM $CaCl_2$ for 15 min. TCNF-ELMs were incubated for 3 days at 25°C under 20 μmol $m^{-2}$ $s^{-1}$

PAR in ambient air. For photobiotransformation experiments, five biological replicates were used, each with 2–4 technical replicates.

### 2.4. Photobiotransformation and gas chromatography

All photobiotransformation reactions were executed in 37 ml vials containing TAP medium (pH 7.2) with a 3–3.25 ml total reaction volume. Reactions were conducted at 25°C with shaking at 90 rpm under 26 μmol $m^{-2}$ $s^{-1}$ PAR provided by a fluorescent lamp (Philips Master TL-D 36 W/865, the Netherlands). The reaction mixture included 5 mM cyclohexanone (Sigma Aldrich, Italy), 25 mM MOPS (Sigma Aldrich, USA), and 1.7% (v/v) ethanol following the best conditions described in [8]. The ELMs were placed in the vials fully submerged in the reaction mixture. For long-term experiments, photobiotransformations were performed by replacing the reaction medium, thereby supplementing it with fresh substrate every 24 h. Samples were collected, extracted with acidified ethyl acetate and analyzed as described in [8] using a gas chromatograph (GC-2010 Pro, Shimadzu, Japan) equipped with a flame ionization detector (FID), AOC-20s auto sampler, AOC-20i auto injector and a HP-5MS 30 m × 0.25 mm (5%-phenyl)-methylpolysiloxane column (19091S-133, Agilent, USA). Nitrogen was used as the carrier gas.

Specific reaction rates were calculated based on the formation of the target compound. Rates were normalized to the initial Chl concentration of the cells entrapped in the ELMs. Additionally, normalization to dry cell weight was performed using a correlation curve derived from the initial Chl content [8].

The formation of ε-caprolactone and cyclohexanol followed a sigmoidal curve, and the maximal reaction velocity was calculated with Origin (OriginLab Corporation, USA) using slogistics2 fitting. Cyclohexanol formation in Alg-ELM did not follow a sigmoidal curve; therefore, a linear fit between time points 1 and 6 h was used. Statistical significance was tested with a homoscedastic *t*-test.

### 2.5. Chlorophyll determination

Alg-ELMs were dissolved in 50 mM EDTA (pH 7.0), after which the recovered cells were collected and resuspended in 94% (v/v) ethanol. The samples were then centrifuged prior to the absorbance measurements. Chl *a*+*b* content was calculated according to [36] by subtracting the absorbance at 720 nm from values at 649 and 665 nm. TCNF-ELMs were dissolved in methanol by incubating for 20 min at + 60°C, followed by overnight storage at + 4°C. Chl content was calculated according to [39]. All absorbance measurements were performed using aUV-1800 spectrophotometer (Shimadzu, Japan).

### 2.6. Photosynthetic activity

Maximum quantum efficiency of Photosystem II (Fv/Fm) was determined using a PAM 2000 Portable Chlorophyll Fluorometer (Walz, Germany). The ELMs were dark adapted for 10 min before the measurement. A light pulse of 0.8 s at 3000 μmol $m^{-2}$ $s^{-1}$ PAR was applied from the top to detect the maximum fluorescence yield (Fm).

## 3. Results and discussion

### 3.1. Whole-cell photobiotransformation in ELMs with entrapped Chlamydomonas

#### 3.1.1. Determining the optimal growth phase for enhanced CHMO expression prior to immobilization

The recombinant *Chlamydomonas* used in this study expresses CHMO under the control of the HSP70A-RBCS2 fusion promoter [8,40]. This promoter is strong under basal conditions and inducible by light, therefore, CHMO accumulation levels may vary across different cultivation phases. To determine the optimal time point for immobilization, cells were sampled over a five-day cultivation period in TAP medium, and the levels of the recombinant enzyme were monitored using an anti-HA antibody specific to the C-terminal 3 ×HA tag fused to CHMO. Our results showed that during the early growth phase (day 0–2), when cell density is low and light penetration is high, the accumulation of the heterologous enzyme peaked, reaching its maximum on day 1 (Fig. 1). No significant difference was observed between days 2 and 3, although CHMO levels on day 3 were significantly lower than on days 1 ($p = 0.03$, corrected using the Benjamini-Hochberg method). The enzyme level declined significantly when cells transitioned into the stationary phase on days 4 and 5. Cells harvested on day 3 were selected for further experiments, as this time point provided a balance of high CHMO accumulation and maximal Chl content, the latter serving as a proxy for biomass.

#### 3.1.2. Photobiotransformation in Chlamydomonas cells entrapped in various ELMs

First, we adopted a previously established protocol for the entrapment of ethylene-producing *Synechocystis* in alginate [29] and applied it to *Chlamydomonas* (A1-Alg-ELM). CHMO converts the fed substrate, cyclohexanone, into ε-caprolactone. However, in addition to the main reaction, *Chlamydomonas* encodes several inherent alcohol dehydrogenases (ADHs), which may catalyze a side reaction, converting cyclohexanone to cyclohexanol (Scheme 1). Through the addition of ethanol and optimization of light conditions, the proportion of this side product was previously reduced to 13% in suspension cultures [8]. In this study, we applied the best conditions identified for suspension cultures to *Chlamydomonas* cells entrapped in A1-Alg-ELM. We observed

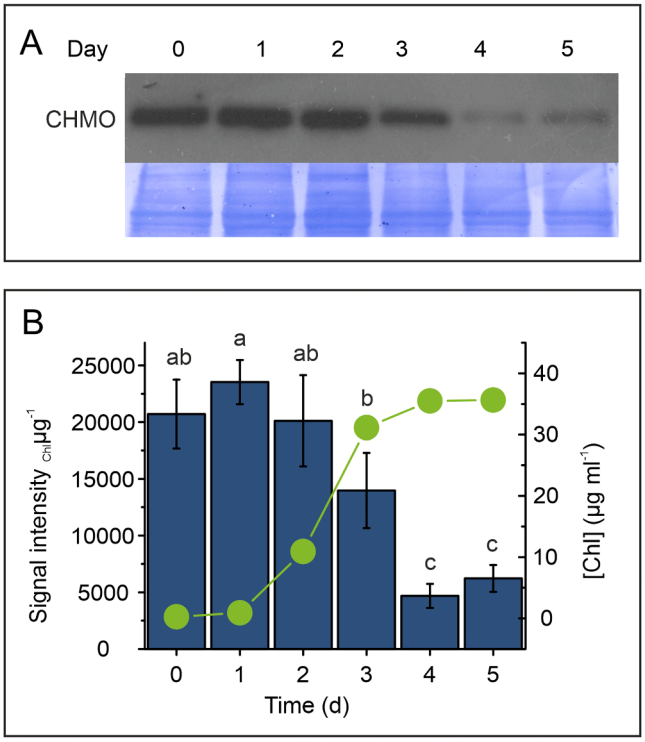


**Fig. 1.** The CHMO expression over a five-day cultivation period. A) Western blot analysis using an HA-specific antibody to detect the CHMO enzyme. Total protein loading was visualized by Coomassie staining. The membrane and the X-ray film images shown are representatives of three independent experiments. B) Quantification of HA signal (reflecting CHMO) intensity normalized to Chl. Additionally the Chl concentration of the sample is shown with green dots (right y-axis). Data present the mean ± standard deviation (n = 3). Statistical significance was assessed using a two-tailed Student's *t*-test assuming equal variance. Multiple comparisons were corrected using the Benjamini-Hochberg False Discovery Rate (FDR) method to control for Type I errors. The individual repetitions are shown in Supplementary Fig. S1.

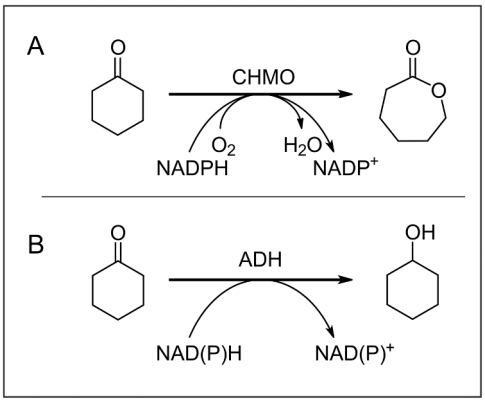


**Scheme 1.** Reactions presented in the work. A) Reaction catalyzed by cyclohexanone monooxygenase (CHMO); cyclohexanone is converted to ε-caprolactone and B) the side reaction catalyzed by alcohol dehydrogenase (ADH); cyclohexanone is converted to cyclohexanol.

that the photobiotransformation reaction, converting 5 mM of fed cyclohexanone to ε-caprolactone, reached completion within 24 h, with an average of 25% side product present (Fig. 2A, D). The reaction had a specific activity of $0.017 \pm 0.005$ $mg_{Chl}^{-1}$ ($1.19 \pm 0.35$ $g_{DCW}^{-1}$) with a maximal volumetric rate of $153.4 \pm 10.5$ μM $h^{-1}$ (Fig. 2A, D–G). Thus, the reaction proceeded slower and produced more side product compared to suspension cultures [8]. Interestingly, despite substantial variations in Chl content among the Alg1-ELM films (Fig. 2E), the reaction rates showed relatively low variability (Fig. 2A, E). This suggests that not all the cells within the films were actively performing the reaction, likely due to cell saturation within the matrix. These findings prompted us to explore different approaches.

Next, we reduced the initial cell loading concentration (designated as A2-Alg-ELM in Mat & Met) to investigate whether lowering cell density within the films could improve reaction efficiency and reduce side product formation. The light conditions were kept the same to evaluate the effect of cell loading, but in addition, the ELMs were incubated for three days before initiating the photobiotransformation. This approach was motivated by previous observations showing that lower cell density combined with a pre-incubation period improves performance when photocured Alg + GGMMA + LAP matrix is used to encapsulate *Chlamydomonas* cells [41], compared to the A1-Alg-ELMs.

The A2-Alg-ELM outperformed A1-Alg-ELMs in the photobiotransformation, exhibiting a 1.4-fold higher maximal reaction rate and reaching $216.10 \pm 14.04$ μM $h^{-1}$. This reaction rate was also higher than that observed for the photocured Alg + GGMMA + LAP films [41]. Additionally, the specific activity of the A2-Alg-ELMs ($0.056 \pm 0.005$ $mg_{Chl}^{-1}$) was comparable to that of the Alg + GGMMA + LAP ($0.051 \pm 0.003$ $mg_{Chl}^{-1}$) [41] and 3.2-fold higher than that of the A1-Alg-ELMs. Furthermore, the A2-Alg-ELMs demonstrated an improved product-to-side product ratio, with side product formation levels averaging to only 7%, along with a significantly lower side product formation rate (Fig. 2B, D–G).

In addition to optimizing cell loading, we fabricated ELMs using TCNF as the matrix material, as TCNF has been demonstrated to outperform alginate in bioproduction [20,35]. The same cell density used for the A2-Alg-ELMs was employed for the TCNF-ELMs. In the TCNF-ELMs, the photobiotransformation reaction proceeded 1.1 times faster ($248.2 \pm 21.4$ μM $h^{-1}$) than in the A2-Alg-ELMs, with a 1.4-fold higher specific activity, reaching $0.078 \pm 0.018$ $mg_{Chl}^{-1}$ ($5.30 \pm 1.25$ $g_{DCW}^{-1}$). The side product-to-product ratio was 11% (Fig. 2C–G). The kinetics of the side product accumulation indicate that the

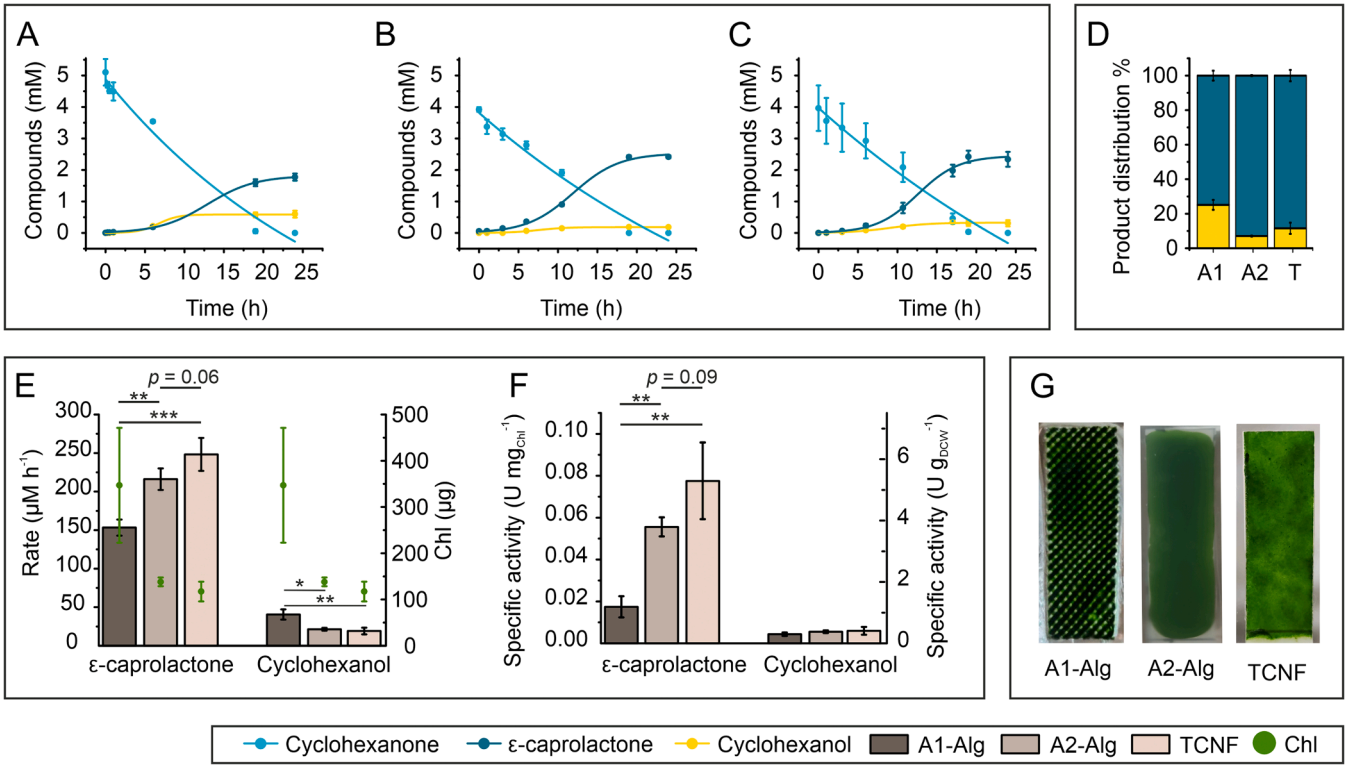


**Fig. 2.** The whole-cell photobiotransformation with different ELMs. Time course of the photobiotransformation using A) A1-Alg-ELMs, B) A2-Alg-ELMs, and C) TCNF-ELMs. D) The product distribution after 24 h of photobiotransformation across the different materials. E) Maximal reaction rates and corresponding Chl content per film. F) The specific activities normalized to Chl and dry cell weight (DCW). G) Photographs of the freshly prepared ELMs. Data represent the mean ± standard deviation from 3 to 4 independent replications. Statistical significance was determined using a two-tailed Student's *t*-test assuming equal variance. * $p < 0.05$, ** $p < 0.005$, *** $p < 0.0005$.

cyclohexanol begins to accumulate after approximately 1 h in A1-Alg-ELMs, and between 3 and 6 h in A2-Alg-ELMs and TCNF-ELMs (Fig. 2). The CHMO reaction follows a sigmoidal kinetic profile, with the maximum reaction rate occurring despite the presence of a measurable amount of side product. These results indicate that, at the concentrations reached in this study, the side product does not impede CHMO activity.

In all tested setups the ELMs remained intact during the overnight reaction and demonstrated higher maximal volumetric reaction rates (Fig. 2E) compared to previously reported values for immobilized *Synechocystis* expressing a BVMO from *Parvibaculum lavamentivorans* DSM 1302332 ($BVMO_{Parvi}$) (60 ± 1 μM $h^{-1}$, [26]) which can be attributed to higher cell loading. $BVMO_{Parvi}$ is known to be a faster enzyme than CHMO [6] and in our setup, the specific activities likewise did not reach the values reported for immobilized $BVMO_{Parvi}$ (0.34–0.35 $mg_{Chl}^{-1}$, Fig. 2F, [26]). The reaction yield did not reach 100% (Fig. 2A–C), which could partially be attributed to the compound-matrix interactions, which may prevent efficient diffusion of compounds out of matrix. A similar phenomenon was observed in earlier experiments with immobilized cells [26].

When comparing the volumetric photoproduction rates obtained in this study with previously reported values for cyanobacterial production systems (typically expressed in mg $h^{-1}$ $L^{-1}$), it becomes evident that the present results are highly competitive. The A1-Alg-ELM, A2-Alg-ELM, and TCNF-ELM systems achieved rates of 17.5 ± 1.2 mg $h^{-1}$ $L^{-1}$, 24.7 ± 1.6 mg $h^{-1}$ $L^{-1}$, 28.3 ± 2.4 mg $h^{-1}$ $L^{-1}$, respectively (Supplementary Fig. S2), exceeding or matching the broad range previously reported for flask-based suspensions (0.06–16 mg $h^{-1}$ $L^{-1}$) [42–50].

### 3.2. Extended whole-cell photobiotransformation in ELMs over multiple reaction cycles

#### 3.2.1. Comparison of Alg-ELMs and TCNF-ELMs in semi-continuous mode

One of the key benefits of immobilization is the separation of biocatalytic cells from the medium (including substrate and product), enabling multiple production cycles without the need to harvest cells. Instead, the surrounding medium can simply be refreshed [29,41]. Recently, natural biofilms composed of mixed microbial species, including *Synechocystis,* have been reported to enable prolonged production of cyclohexanol from cyclohexane, catalyzed by a cytochrome P450 monooxygenase [25,51]. Similarly, natural biofilms formed by heterotrophic bacteria, such as *Pseudomonas taiwanensis* engineered to express a BVMO, have also been exploited for biotransformation [52]. However, to the best of our knowledge, no reports have demonstrated prolonged photobiotransformation using highly controllable photosynthetic ELMs – defined in terms of cell type, film thickness and cell density – composed of living cells encapsulated within tailored scaffold materials. Next, we evaluated the feasibility of multiple cycles of CHMO-driven photobiotransformation.

We compared the performance of the A2-Alg-ELMs and TCNF-ELMs over multiple photobiotransformation cycles using a semi-continuous operational mode, where the immobilized cells remained within the films, while the surrounding medium was replaced every 24 h with fresh substrate, simultaneously removing the accumulated product. Both types of ELMs supported repeated cycles of photobiotransformation, but the TCNF-ELMs gradually lost structural integrity and disintegrated during the seven-day experiment, while the A2-Alg-ELMs remained intact throughout the operational period (Supplementary Fig. S3–S4). The disintegration of the TCNF-ELMs occurred at different time points, some disintegrating already after the second cycle, while others remained intact for a longer period and disintegrated after the fourth cycle. However, none of the TCNF films remained intact by the end of the seven-day experiment. The variability of the mechanical stability of the films resulted in high variability between samples and led to a lower overall product yield compared to the A2-Alg-ELMs. Over the course of seven days, A2-Alg-ELMs produced a cumulative ε-caprolactone yield of 0.15 mol $m^{-2}$, while TCNF-ELMs yielded only 0.06 mol $m^{-2}$ (Fig. 3A–B).

To assess the photosynthetic activity of the ELMs during the long-term production phase, we measured the maximum quantum efficiency of Photosystem II (Fv/Fm). The measurements were conducted using the ELMs incubated in the biotransformation mix, which was refreshed daily. As a control, ELMs incubated in TAP medium, refreshed every 1–4 days, were used. The photosynthetic activity of cells in the A2-Alg-ELMs incubated with the biotransformation mix remained stable until day 9 after immobilization, corresponding to day 6 of the photobiotransformation experiment (following 2 days acclimation in the films prior to initiating biotransformation, Fig. 3C). In contrast, in the TCNF-ELMs, photosynthetic activity started to decline on the second day of photobiotransformation (day 5 after immobilization). This decrease mirrored the reduction in photobiotransformation performance (Figs. 3D, 3B).

In the control experiments with TAP-medium, without the biotransformation mixture, the cells embedded in either materials, alginate or TCNF, showed stable photosynthetic activity during the first week. After this period, a slight decline in activity was observed in TCNF-embedded cells, while alginate-embedded cells remained photosynthetically active for up to 14 days, after which a slight decline was detectable (Fig. 3C–D).

As the photosynthetic activity remains high in the A2-Alg-ELMs in TAP-medium, the main contributor to the decline in photosynthetic activity of alginate embedded cells seems to be the compounds present in the biotransformation mix in addition to TAP medium, including MOPS-buffer, ethanol, the substrate and the reaction products. Ethanol, at the concentration applied here (1.7% v/v), is known to negatively impact *Chlamydomonas* growth [53]. Moreover, we have previously shown that both the substrate and product influence cell growth and oxygen evolution [8]. Therefore, it is not surprising that prolonged exposure to the biotransformation mix results in a gradual decline in photosynthetic activity, as observed in our experiments.

Previously, TCNF-cyanobacteria films were reported to exhibit somewhat higher porosity and better rheological properties in terms of yield stress, critical stress and viscoelastic stability compared to alginate [54]. Furthermore, the TCNF-films manifested superior stability over alginate films for ethylene production in a high ionic strength medium. In that study, the addition of 200 mM bicarbonate caused rapid disintegration of calcium-crosslinked alginate films, while TCNF films remained intact [35]. However, in that setup, the films were neither shaken nor exposed to frequent medium exchange, which significantly reduces mechanical stress. In contrast, our experiments required continuous shaking and regular medium refreshing, both essential for photobiotransformation, as they ensure sufficient substrate delivery and product removal. Importantly, our system did not rely on high ionic strength conditions, which were previously shown to compromise alginate stability. Our results suggest that mechanical stress is particularly detrimental to TCNF-ELM stability, while in static, high ionic strength environments, TCNF-ELMs outperform alginate-based alternatives.

In our study, lower cell loading in A2-Alg-ELMs resulted in faster reaction rates and higher specific activity (Fig. 2). This contrasts with recent findings using *Synechocystis* expressing $BVMO_{Parvi}$, where a lower cell amount (14.66 μg Chl immobilized vs. $OD_{750}$=25) led to slower reaction rates [6,26]. We hypothesize that in both published $BVMO_{Parvi}$ systems, cells were still operating under conditions with sufficient light exposure. In contrast, while the surface cells in the A1-Alg films still received sufficient light, the high cell density likely caused light limitation for cells deeper in the matrix, causing significant slowdown of the CHMO reaction. When further comparing our results to published data, the specific activity of A2-Alg-ELMs was comparable to the Alg + GGMMA + LAP films [41]. However, our system exhibited a higher maximal volumetric reaction rate. This suggests that our ELMs operate close to an optimal range of cell loading, where a slight increase in cell concentration can enhance the overall reaction rate without

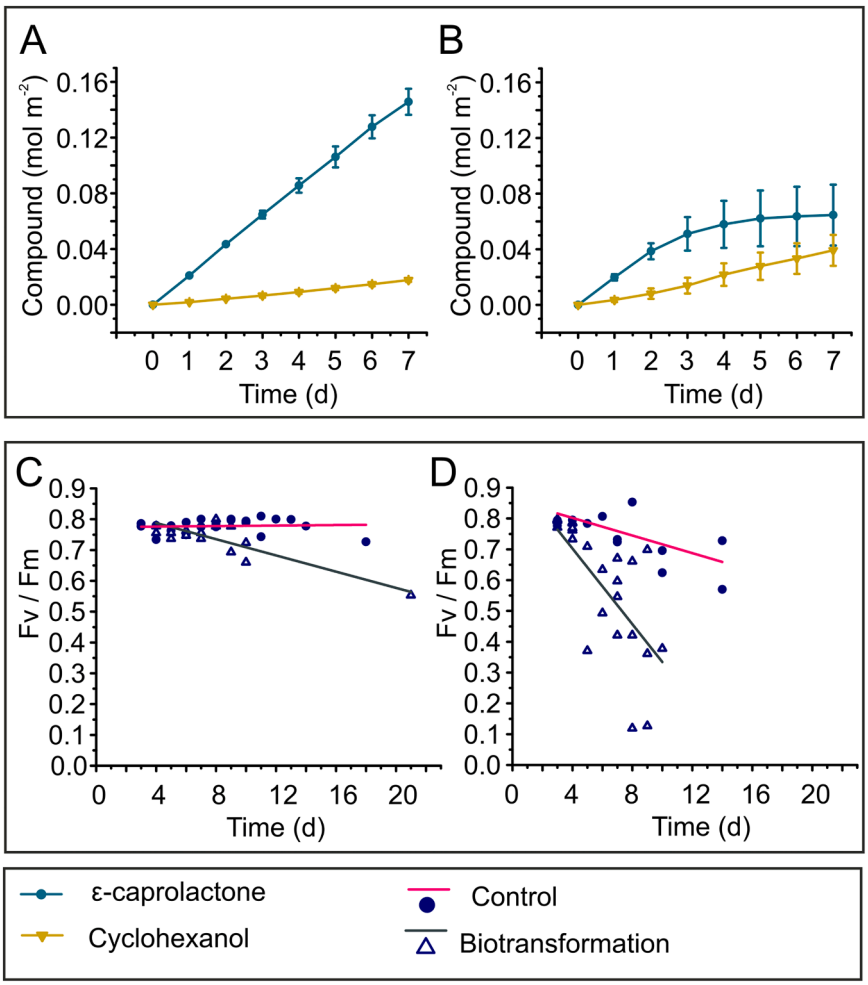


**Fig. 3.** Semi-continuous photobiotransformation in A2-Alg-ELMs and TCNF-ELMs. The biotransformation mix was sampled and replaced every 24 h. A) The cumulative conversion of cyclohexanone to ε-caprolactone and cyclohexanol over seven days using A2-Alg-ELMs (9 films from 3 independent trials). B) The cumulative conversion of cyclohexanone to ε-caprolactone and cyclohexanol over seven days using TCNF-ELMs (9 films from 3 independent trials). C) The photosynthetic activity of A2-Alg-ELMs and D) TCNF-ELMs during semi-continuous biotransformation. The blue circles with pink lines refer to control ELMs incubated in pure TAP-medium. Blue triangles with blue lines refer to ELMs incubated in the daily refreshed biotransformation mix. The lines are averages of the results.

significantly compromising the activity of individual cells within the ELM.

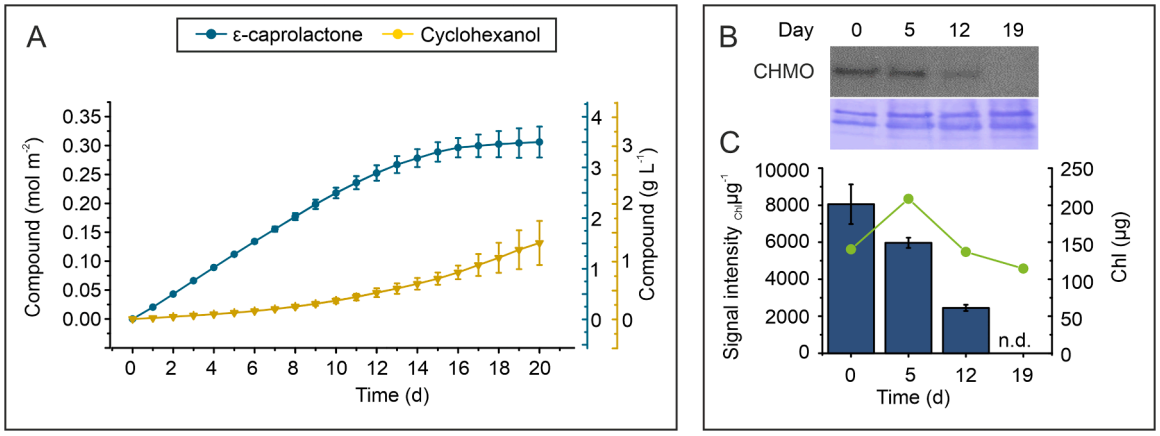


**Fig. 4.** Semi-continuous photobiotransformation in A2-Alg-ELMs A) The cumulative conversion of cyclohexanone to ε-caprolactone and cyclohexanol over 20 days using A2-Alg-ELMs (3 independent films). B) Western blot analysis of the films at different time points using an HA-specific antibody to detect the CHMO enzyme. Total protein loading was visualized by Coomassie staining. The membrane and the X-ray film images shown are representatives of three independent experiments. seven days using TCNF-ELMs (9 films from 3 independent trials). C) Quantification of HA signal (reflecting CHMO) intensity normalized to Chl. Additionally the Chl concentration of the sample is shown with green dots (right y-axis). Data present the mean ± standard deviation (n = 3). The individual repetitions are shown in Supplementary Fig. S7.

*3.2.2. Extending the semi-continuous biotransformation in Alg-ELMs*

We next extended the photobiotransformation cycles in the A2-Alg-ELMs beyond the initial seven-day period, as the films remained structurally intact throughout the experiment. Product formation continued linearly over two weeks, reaching a cumulative yield of 0.31 ± 0.03 mol $m^{-2}$ after 20 days (Fig. 4A), corresponding to 34.93 ± 3.05 g $m^{-2}$. This translates to a volumetric yield of 3.49 ± 0.31 g $L^{-1}$. Direct comparison with previously reported values is challenging, due to variability in expressed enzymes, including catalytic activity, host organisms, and reactor configurations in whole–cell photobiotransformation [11,18,19,25,55,56].

Nevertheless, we provide here a contextual positioning of our results. The volumetric yield achieved in this study (3.49 ± 0.31 g $L^{-1}$) is comparable to that of an engineered *Synechocystis* strain expressing a BVMO from *Acidovorax* sp. CHX100, which yielded 1.3 ± 0.1 g $L^{-1}$ of ε-caprolactone within 27 h in stirred-tank fed-batch mode [18]. When the reaction was coupled to a lactonase, the system reached titers 3.11 ± 0.12 g $L^{-1}$ of 6-hydroxyhexanoic acid in 48 h [19]. Although the product levels obtained in the current study fall within the same order of magnitude as these state-of-the-art suspension biotransformations, they accumulated over a much longer period. This extended time requirement is expected, as the semi-continuous ELM configuration operates at a slower reaction rate than fed-batch suspension culture. Nevertheless, the long-term stability of the ELMs suggests that in the future they could be used in a continuous approach to reach higher overall productivity.

The average area-based productivity of A2-Alg-ELMs during the 20-day experiment was 2.31 ± 0.25 g $m^{-2}$ $d^{-1}$, which is comparable in magnitude to that reported for mixed-species films with *Synechocystis* expressing a cytochrome P450 monooxygenase (3.76 g $m^{-2}$ $d^{-1}$) [51], but slower than that of a natural biofilm composed of a heterotrophic *P. taiwanensis* expressing a BVMO (prolonged rate 14 g $m^{-2}$ $d^{-1}$) [52].

When considering the long-term volumetric productivity, the average rate of 9.64 ± 1.08 mg $h^{-1}$ $L^{-1}$ measured for the A2-Alg-ELM (Supplementary Fig. S5) falls within the range reported for cyanobacterial suspension cultures in flasks (0.06–16 mg $h^{-1}$ $L^{-1}$) [55]. The reaction rates may be potentially improved using dedicated photobioreactor configurations, such as a continuous coil reactor operating with *Synechocystis* expressing a fast BVMO from *Burkholderia xenovorans* [6] achieved a seven-fold improvement over batch cultivation, reaching a space-time-yield of 2.8 g $L^{-1}$ $h^{-1}$ [56]. It should be noted, however, that although the reactor flow was continuous, the production was not continuous, as the substrate was not periodically added, but given only at the beginning of the experiment.

The best performing A2-Alg-ELMs continued accumulating product up to day 20, reaching a cumulative yield of 0.34 mol $m^{-2}$, comparable to yields reported for molecular hydrogen production with immobilized wild-type *Chlamydomonas* [20]. During the long-term experiment, side product formation remained below 10% for the first 4 days before gradually increasing thereafter (Fig. 4A).

Disintegration of the A2-Alg-ELMs started after 13 cycles of photobiotransformations with films fragmenting into smaller pieces. This coincided with the incomplete turnover of the substrate within the 24-hour reaction timescale (Supplementary Fig. S6). Notably, similar disintegration was also observed in control ELMs without the biotransformation mix, suggesting that the effect is primarily related to matrix stability rather than the biotransformation reaction-specific. Notably, one film remained completely intact for 20 consecutive cycles (Supplementary Fig. S3), demonstrating the potential for long-term operation with further optimization. In addition to shaking, the repeated medium exchanges likely contributed to mechanical stress on the ELMs during prolonged production process.

To understand why product formation did not continue linearly even if the films remained intact, we investigated the expression of CHMO in the cells embedded within films. Samples were collected at the start of the biotransformation and after 5, 12 and 19 days of semi-continuous production. The amount of CHMO normalized per Chl declined over time: after 5 days, CHMO amount decreased to 74% of the initial amount; by the day 12, only 30% remained; and by day 19, CHMO was below the detection limit (Fig. 4B–C). The Chl amount within the films increased to about 1.5 times the initial on day 5 of biotransformation after which the Chl declined close to the original value on day 12 and by the end of the experiment the value was about 80% of the original value (Fig. 4C). Based on the results, the cell growth within the ELMs was in agreement with the photosynthetic activity (Fig. 3C).

The gradual decline of the CHMO level coincides with increasing accumulation of the side product at the expense of the desired product. As CHMO levels decline, the substrate becomes more available to the inherent ADH enzymes, that convert it to the side product.

Similar instability of the CHMO enzyme has been reported in *E. coli* [57], which was attributed to low levels of cofactors required for stabilizing the enzyme [16]. However, in *E. coli*, the decline in CHMO occurred in hour-time scale whereas in *Chlamydomonas* the decline was much slower, suggesting additional factors influence enzyme levels in this system. *Chlamydomonas* is widely recognized for its challenges in heterologous gene expression, often due to transgene silencing mechanisms [58]. The background strain used in this study (UVM11-CW), which possesses a mutation in histone deacetylase, exhibits improved transgene expression capacity and has been shown to stably express yellow fluorescent protein (YFP) for over two years [59]. We cannot exclude the possibility that maintaining the immobilized strain without antibiotics during production phase might remove selection pressure, potentially leading to reduced protein expression. However, our recent study using an ethylene-producing cyanobacteria strain immobilized in films demonstrated remarkable stability for nearly four months, suggesting that immobilization—by restricting cell growth and reducing resource trade-offs—may, in fact, contribute to genetic stability [31]. Moreover, factors contributing to transgene silencing could also arise from post-transcriptional regulations. These aspects necessitate further investigation, alongside studies aimed at improving robustness of the ELMs and at examining how cell density, spatial distribution, and light availability influence biotransformation efficiency, as quantitative insight into these parameters would support process optimization and scale-up.

## 4. Conclusion

We established a proof-of-the concept for sustained CHMO-driven photobiotransformation using engineered *Chlamydomonas* embedded in alginate based ELMs, maintained for over two weeks in a semi-continuous production mode. The successful implementation of multiple reaction cycles highlights the potential applicability of photosynthetic ELMs for long-term photobiotransformation thereby providing a basis for the development of large scale continuous flow photobioreactor concepts. Furthermore, this approach is adaptable to other engineered microorganisms, expanding its relevance to a broad range of biocatalytic applications.

## CRediT authorship contribution statement

**Yagut Allahverdiyeva:** Writing – review & editing, Resources, Project administration, Investigation, Funding acquisition, Conceptualization. **Tekla Tammelin:** Writing – review & editing, Resources, Funding acquisition. **Pornpan Napaumpaiporn:** Investigation, Formal analysis. **Tiia Siivola:** Writing – review & editing, Investigation, Formal analysis. **Vilja Siitonen:** Writing – original draft, Supervision, Methodology, Investigation, Formal analysis.

## Declaration of Competing Interest

The authors declare that they have no known competing financial interests or personal relationships that could have appeared to influence the work reported in this paper.

## Acknowledgments

This work was supported by the EU FET Open project "FuturoLEAF" (grant agreement no. 899576), the Research Council of Finland "Alga-LEAF" (project no. 322752 and 322754), the Novo Nordisk Foundation project "PhotoCat" (project no. NNF20OC0064371 to YA) and Jane and Aatos Erkko Foundation project "PhotoFactory" (project no. 230042 to YA); and the Research Council of Finland's Flagship Programme (Competence Centre for Materials Bioeconomy, FinnCERES). The work was carried out using the PHOTOSYN infrastructure at the University of Turku.

## Appendix A. Supporting information

Supplementary data associated with this article can be found in the online version at doi:10.1016/j.nbt.2026.04.004.

## Data availability

Data will be made available on request.

## References

[1] Nikkanen L, Hubáček M, Allahverdiyeva Y. Photosynthesis: biotechnological applications with microalgae. Berlin: De Gruyter; 2021. https://doi.org/10.1515/9783110716979.
[2] Malihan-Yap L, Grimm HC, Kourist R. Recent advances in cyanobacterial biotransformations. Chem Ing Tech 2022;94:1628–44. https://doi.org/10.1002/cite.202200077.
[3] Böhmer S, Marx C, Gómez-Baraibar Á, Nowaczyk MM, Tischler D, Hemschemeier A, et al. Evolutionary diverse *Chlamydomonas reinhardtii* Old Yellow Enzymes reveal distinctive catalytic properties and potential for whole-cell biotransformations. Algal Res 2020;50:101970. https://doi.org/10.1016/j.algal.2020.101970.
[4] Assil-Companioni L, Büchsenschütz HC, Solymosi D, Dyczmons-Nowaczyk NG, Bauer KKF, Wallner S, et al. Engineering of NADPH supply boosts photosynthesis-driven biotransformations. ACS Catal 2020;10:11864–77. https://doi.org/10.1021/acscatal.0c02601.
[5] Böhmer S, Köninger K, Gómez-Baraibar Á, Bojarra S, Mügge C, Schmidt S, et al. Enzymatic oxyfunctionalization driven by photosynthetic water-splitting in the cyanobacterium *Synechocystis* sp. PCC 6803. Catalysts 2017;7:240. https://doi.org/10.3390/catal7080240.
[6] Erdem E, Malihan-Yap L, Assil-Companioni L, Grimm H, Barone GD, Serveau-Avesque C, et al. Photobiocatalytic oxyfunctionalization with high reaction rate using a Baeyer−Villiger monooxygenase from *Burkholderia xenovorans* in metabolically engineered cyanobacteria. ACS Catal 2022;12:66–72. https://doi.org/10.1021/acscatal.1c04555.
[7] Mascia F, Pereira SB, Pacheco CC, Oliveira P, Solarczek J, Schallmey A, et al. Light-driven hydroxylation of testosterone by *Synechocystis* sp. PCC 6803 expressing the heterologous CYP450 monooxygenase CYP110D1. Green Chem 2022;24:6156–67. https://doi.org/10.1039/d1gc04714k.
[8] Siitonen V, Probst A, Tóth G, Kourist R, Schroda M, Kosourov S, et al. Engineered green alga *Chlamydomonas reinhardtii* as a whole-cell photosynthetic biocatalyst for stepwise photoproduction of $H_2$ and ε-caprolactone. Green Chem 2023;25:5945–55. https://doi.org/10.1039/d3gc01400b.
[9] Bretschneider L, Heuschkel I, Ahmed A, Bühler K, Karande R, Bühler B. Characterization of different biocatalyst formats for BVMO-catalyzed cyclohexanone oxidation. Biotechnol Bioeng 2021;118:2719–33. https://doi.org/10.1002/bit.27791.
[10] Hoschek A, Toepel J, Hochkeppel A, Karande R, Bühler B, Schmid A. Light-dependent and aeration-independent gram-scale hydroxylation of cyclohexane to cyclohexanol by CYP450 harboring *Synechocystis* sp. PCC 6803. Biotechnol J 2019;14:1800724. https://doi.org/10.1002/biot.201800724.
[11] Hubáček M, Nikkanen L, Allahverdiyeva Y. Optimising $CO_2$ level and light quality for enhanced whole-cell biotransformation reactions in *Synechocystis* sp. PCC 6803. Micro Cell Fact 2025;24:198. https://doi.org/10.1186/s12934-025-02828-4.
[12] Lin B, Tao Y. Whole-cell biocatalysts by design. Micro Cell Fact 2017;16:106. https://doi.org/10.1186/s12934-017-0724-7.
[13] Leisch H, Morley K, Lau PCK. Baeyer−Villiger monooxygenases: more than just green chemistry. Chem Rev 2011;111:4165–222. https://doi.org/10.1021/cr1003437.
[14] Tolmie C, Smit MS, Opperman DJ. Native roles of Baeyer–Villiger monooxygenases in the microbial metabolism of natural compounds. Nat Prod Rep 2019;36:326–53. https://doi.org/10.1039/c8np00054a.
[15] Hilker I, Baldwin C, Alphand V, Furstoss R, Woodley J, Wohlgemuth R. On the influence of oxygen and cell concentration in an SFPR whole cell biocatalytic Baeyer-Villiger oxidation process. Biotechnol Bioeng 2006;93:1138–44. https://doi.org/10.1002/bit.20829.
[16] Milker S, Goncalves LCP, Fink MJ, Rudroff F. *Escherichia coli* fails to efficiently maintain the activity of an important flavin monooxygenase in recombinant overexpression. Front Microbiol 2017;8:2201. https://doi.org/10.3389/fmicb.2017.02201.
[17] Cabadaj P, Illeová V, Červeňanský I, Rupčíková V, Krajčovič T, Bučko M, et al. Investigation of process stability of a whole-cell biocatalyst with Baeyer-Villiger monooxygenase activity in continuous bioreactors. Environ Technol Innov 2023;30:103083. https://doi.org/10.1016/j.eti.2023.103083.
[18] Tüllinghoff A, Uhl MB, Nintzel FEH, Schmid A, Bühler B, Toepel J. Maximizing photosynthesis-driven Baeyer–Villiger oxidation efficiency in recombinant *Synechocystis* sp. PCC6803. Front Catal 2022;1:780474. https://doi.org/10.3389/fctls.2021.780474.
[19] Tüllinghoff A, Djaya-Mbissam H, Toepel J, Bühler B. Light-driven redox biocatalysis on gram-scale in *Synechocystis* sp. PCC 6803 via an *in vivo* cascade. Plant Biotechnol J 2023;21:2074–83. https://doi.org/10.1111/pbi.14113.
[20] Kosourov S, Tammelin T, Allahverdiyeva Y. Engineered biocatalytic architecture for enhanced light utilisation in algal $H_2$ production. Energy Environ Sci 2025;18:937–47. https://doi.org/10.1039/d4ee03075c.
[21] Giannelli L, Scoma A, Torzillo G. Interplay between light intensity, chlorophyll concentration and culture mixing on the hydrogen production in sulfur-deprived *Chlamydomonas reinhardtii* cultures grown in laboratory photobioreactors. Biotechnol Bioeng 2009;104:76–90. https://doi.org/10.1002/bit.22384.
[22] Pruvost J, Le Borgne F, Artu A, Legrand J. Development of a thin-film solar photobioreactor with high biomass volumetric productivity (AlgoFilm©) based on process intensification principles. Algal Res 2017;21:120–37. https://doi.org/10.1016/j.algal.2016.10.012.
[23] Valotta A, Malihan-Yap L, Hinteregger K, Kourist R, Gruber-Woelfler H. Design and investigation of a photocatalytic setup for efficient biotransformations within recombinant cyanobacteria in continuous flow. ChemSusChem 2022;15:e202201468. https://doi.org/10.1002/cssc.202201468.
[24] Zou N, Richmond A. Effect of light-path length in outdoor flat plate reactors on output rate of cell mass and of EPA in *Nannochloropsis* sp. J Biotechnol 1999;70:351–6. https://doi.org/10.1016/S0168-1656(99)00087-5.
[25] Bozan M, Berreth H, Lindberg P, Bühler K. Cyanobacterial biofilms: from natural systems to applications. Trends Biotechnol 2025;43:318–32. https://doi.org/10.1016/j.tibtech.2024.08.005.
[26] Arumughan V, Medipally H, Torris A, Levä T, Grimm HC, Tammelin T, et al. Bioinspired nanochitin-based porous constructs for light-driven whole-cell biotransformations. Adv Mat 2025;37:2413058. https://doi.org/10.1002/adma.202413058.
[27] Jämsä M, Kosourov S, Rissanen V, Hakalahti M, Pere J, Ketoja JA, et al. Versatile templates from cellulose nanofibrils for photosynthetic microbial biofuel production. J Mater Chem A 2018;6:5825–35. https://doi.org/10.1039/c7ta11164a.
[28] Kosourov S, Leino H, Murukesan G, Lynch F, Sivonen K, Tsygankov AA, et al. Hydrogen photoproduction by immobilized $N_2$-fixing cyanobacteria: understanding the role of the uptake hydrogenase in the long-term process. Appl Environ Microbiol 2014;80:5807–17. https://doi.org/10.1128/aem.01776-14.
[29] Vajravel S, Sirin S, Kosourov S, Allahverdiyeva Y. Towards sustainable ethylene production with cyanobacterial artificial biofilms. Green Chem 2020;22:6404–14. https://doi.org/10.1039/d0gc01830a.
[30] Kadisch M, Willrodt C, Hillen M, Bühler B, Schmid A. Maximizing the stability of metabolic engineering-derived whole-cell biocatalysts. Biotechnol J 2017;12:1600170. https://doi.org/10.1002/biot.201600170.
[31] Kosourov S, Siitonen V, Tóth G, Levä T, Tammelin T, Kallio P, et al. Over four months ethylene production Unlocking potential solid-state photosynthetic cell factories. bioRxiv preprint 2025. https://doi.org/10.1101/2025.09.12.675104.
[32] Fukuzumi H, Saito T, Iwata T, Kumamoto Y, Isogai A. Transparent and high gas barrier films of cellulose nanofibers prepared by TEMPO-mediated oxidation. Biomacromolecules 2008;10:162–5. https://doi.org/10.1021/bm801065u.
[33] Giz AS, Berberoglu M, Bener S, Aydelik-Ayazoglu S, Bayraktar H, Alaca BE, et al. A detailed investigation of the effect of calcium crosslinking and glycerol plasticizing on the physical properties of alginate films. Int J Biol Macromol 2020;148:49–55. https://doi.org/10.1016/j.ijbiomac.2020.01.103.
[34] Painter TJ. Algal polysaccharides. Aspinall GO, editor. The polysaccharides. New York: Elsevier; 1983. p. 195–285.
[35] Rissanen V, Vajravel S, Kosourov S, Arola S, Kontturi E, Allahverdiyeva Y, et al. Nanocellulose-based mechanically stable immobilization matrix for enhanced ethylene production: a framework for photosynthetic solid-state cell factories. Green Chem 2021;23:3715–24. https://doi.org/10.1039/d1gc00502b.
[36] Harris EH. The *Chlamydomonas* sourcebook: A comprehensive guide to biology and laboratory use. New York: Elsevier Science; 1989.
[37] Hammel A, Sommer F, Zimmer D, Stitt M, Mühlhaus T, Schroda M. Overexpression of sedoheptulose-1,7-bisphosphatase enhances photosynthesis in *Chlamydomonas reinhardtii* and has no effect on the abundance of other Calvin-Benson cycle enzymes. Front Plant Sci 2020;11:868. https://doi.org/10.3389/fpls.2020.00868.
[38] Saito T, Nishiyama Y, Putaux JL, Vignon M, Isogai A. Homogeneous suspensions of individualized microfibrils from TEMPO-catalyzed oxidation of native cellulose. Biomacromolecules 2006;7:1687–91. https://doi.org/10.1021/bm060154s.
[39] Porra RJ, Thompson WA, Kriedemann PE. Determination of accurate extinction coefficients and simultaneous equations for assaying chlorophylls a and b extracted with four different solvents: verification of the concentration of chlorophyll standards by atomic absorption spectroscopy. Biochim Biophys Acta Bioenerg 1989;975:384–94. https://doi.org/10.1016/s0005-2728(89)80347-0.

[40] Schroda M, Blöcker D, Beck CF. The HSP70A promoter as a tool for the improved expression of transgenes in *Chlamydomonas*. Plant J 2000;21:121–31. https://doi.org/10.1046/j.1365-313x.2000.00652.x.
[41] Tóth GS, Backman O, Siivola T, Xu W, Kosourov S, Siitonen V, et al. Employing photocurable biopolymers to engineer photosynthetic 3D-printed living materials for production of chemicals. Green Chem 2024;26:4032–42. https://doi.org/10.1039/D3GC04264B.
[42] Gao Z, Zhao H, Li Z, Tan X, Lu X. Photosynthetic production of ethanol from carbon dioxide in genetically engineered cyanobacteria. Energy Environ Sci 2012;5:9857–65. https://doi.org/10.1039/c2ee22675h.
[43] Kukil K, Lindberg P. Metabolic engineering of *Synechocystis* sp. PCC 6803 for the improved production of phenylpropanoids. Micro Cell Fact 2024;23:57. https://doi.org/10.1186/S12934-024-02330-3.
[44] Liu X, Miao R, Lindberg P, Lindblad P. Modular engineering for efficient photosynthetic biosynthesis of 1-butanol from $CO_2$ in cyanobacteria. Energy Environ Sci 2019;12:2765–77. https://doi.org/10.1039/c9ee01214a.
[45] Matsudaira A, Hoshino Y, Uesaka K, Takatani N, Omata T, Usuda Y. Production of glutamate and stereospecific flavors, (*S*)-linalool and (+)-valencene, by *Synechocystis* sp. PCC6803. J Biosci Bioeng 2020;130:464–70. https://doi.org/10.1016/j.jbiosc.2020.06.013.
[46] Miao R, Xie H, Lindblad P. Enhancement of photosynthetic isobutanol production in engineered cells of *Synechocystis* PCC 6803. Biotechnol Biofuels 2018;11:267. https://doi.org/10.1186/S13068-018-1268-8.
[47] Rodrigues JS, Lindberg P. Metabolic engineering of *Synechocystis* sp. PCC 6803 for improved bisabolene production. Metab Eng Commun 2021;12:e00159. https://doi.org/10.1016/j.mec.2020.e00159.
[48] Rueda E, Altamira-Algarra B, García J. Process optimization of the polyhydroxybutyrate production in the cyanobacteria *Synechocystis* sp. and *Synechococcus* sp. Bioresour Technol 2022;356:127330. https://doi.org/10.1016/j.biortech.2022.127330.
[49] Touloupakis E, Rontogiannis G, Silva Benavides AM, Cicchi B, Ghanotakis DF, Torzillo G. Hydrogen production by immobilized *Synechocystis* sp. PCC 6803. Int J Hydrog Energy 2016;41:15181–6. https://doi.org/10.1016/j.ijhydene.2016.07.075.
[50] Veetil VP, Angermayr SA, Hellingwerf KJ. Ethylene production with engineered *Synechocystis* sp. PCC 6803 strains. Micro Cell Fact 2017;16:34. https://doi.org/10.1186/S12934-017-0645-5.
[51] Hoschek A, Heuschkel I, Schmid A, Bühler B, Karande R, Bühler K. Mixed-species biofilms for high-cell-density application of *Synechocystis* sp. PCC 6803 in capillary reactors for continuous cyclohexane oxidation to cyclohexanol. Bioresour Technol 2019;282:171–8. https://doi.org/10.1016/j.biortech.2019.02.093.
[52] Heuschkel I, Hanisch S, Volke DC, Löfgren E, Hoschek A, Nikel PI, et al. *Pseudomonas taiwanensis* biofilms for continuous conversion of cyclohexanone in drip flow and rotating bed reactors. Eng Life Sci 2021;21:258–69. https://doi.org/10.1002/elsc.202000072.
[53] Jiang Y, Xiao P, Shao Q, Qin H, Hu Z, Lei A, et al. Metabolic responses to ethanol and butanol in *Chlamydomonas reinhardtii*. Biotechnol Biofuels 2017;10:1–16. https://doi.org/10.1186/s13068-017-0931-9.
[54] Levä T, Rissanen V, Nikkanen L, Siitonen V, Heilala M, Phiri J, et al. Mapping nanocellulose- and alginate-based photosynthetic cell factory scaffolds: interlinking porosity, wet strength, and gas exchange. Biomacromolecules 2023;24:3484–97. https://doi.org/10.1021/acs.biomac.3c00261.
[55] Grimm HC, Erlsbacher P, Medipally H, Malihan-Yap L, Sovic L, Zöhrer J, et al. Towards high atom economy in whole-cell redox biocatalysis: up-scaling light-driven cyanobacterial ene-reductions in a flat panel photobioreactor. Green Chem 2025;27:2907–20. https://doi.org/10.1039/d4gc05686h.
[56] Malihan-Yap L, Liang Q, Valotta A, Alphand V, Gruber-Woelfler H, Kourist R. Light-driven photobiocatalytic oxyfunctionalization in a continuous reactor system without external oxygen supply. ACS Sustain Chem Eng 2025;13:3939–50. https://doi.org/10.1021/acssuschemeng.4c08560.
[57] Walton AZ, Stewart JD. Understanding and improving NADPH-dependent reactions by nongrowing *Escherichia coli* cells. Biotechnol Prog 2004;20:403–11. https://doi.org/10.1021/bp030044m.
[58] Cerutti H, Johnson AM, Gillham NW, Boynton JE. Epigenetic silencing of a foreign gene in nuclear transformants of *Chlamydomonas*. Plant Cell 1997;9:925–45. https://doi.org/10.1105/tpc.9.6.925.
[59] Neupert J, Gallaher SD, Lu Y, Strenkert D, Segal N, Barahimipour R, et al. An epigenetic gene silencing pathway selectively acting on transgenic DNA in the green alga *Chlamydomonas*. Nat Commun 2020;11:6269. https://doi.org/10.1038/s41467-020-19983-4.